Journal of Magnetic Resonance 214 (2012) 29–41

Contents lists available at SciVerse ScienceDirect

Journal of Magnetic Resonance

journal homepage: www.elsevier.com/locate/jmr

Theoretical aspects of dynamic nuclear polarization in the solid state – The cross effect

Yonatan Hovav *, Akiva Feintuch, Shimon Vega

Department of Chemical Physics, Weizmann Institute of Science, Rehovot, Israel

ARTICLE INFO

Article history:
Received 16 June 2011
Revised 18 September 2011
Available online 5 October 2011

Keywords:
Dynamic Nuclear Polarization (DNP)
NMR
Solid effect
Cross effect

ABSTRACT

In recent years Dynamic Nuclear Polarization (DNP) signal enhancement techniques have become an important and integral part of modern NMR and MRI spectroscopy. The DNP mechanisms transferring polarization from unpaired electrons to the nuclei in the sample is accomplished by microwave (MW) irradiation. For solid samples a distinction is made between three main enhancement processes: Solid Effect (SE), Cross Effect (CE) and Thermal Mixing (TM) DNP. In a recent study we revisited the solid state SE-DNP mechanism at high magnetic fields, using a spin density operator description involving spin relaxation, for the case of an isolated electron spin interacting with neighboring nuclei. In this publication we extend this study by considering the hyper-polarization of nuclei in systems containing two interacting electrons. In these spin systems both processes SE-DNP and CE-DNP are simultaneously active. As previously, a quantum description taking into account spin relaxation is used to calculate the dynamics of spin systems consisting of interacting electron pairs coupled to (core) nuclei. Numerical simulations are used to demonstrate the dependence of the SE- and CE-DNP enhancements on the MW irradiation power and frequency, on electron, nuclear and cross relaxation mechanisms and on the spin interactions. The influence of the presence of many nuclei on the hyper-polarization of an individual core nucleus is examined, showing the similarities between the two DNP processes. These studies also indicate the advantages of the CE- over the SE-DNP processes, both driving the polarization of the bulk nuclei, *via* the nuclear dipole–dipole interactions.

1. Introduction

Solid DNP is currently considered a very promising technique for enhancing sensitivity both for solid-state NMR and for liquid NMR through dissolution [1–4]. In a typical DNP setup the samples include a small concentration of free radicals whose high electron spin polarization is transferred by microwave (MW) irradiation to the nuclei in the sample, resulting in significant enhancements of the NMR signal of the bulk.

DNP in solids transfers polarization from the electron spins to the nuclear spins via the hyperfine interaction. This polarization transfer can result from three different mechanisms: (i) In the solid effect (SE) [5,6] the polarization of a single electron is transferred to its surrounding nuclei. This transfer is a result of MW irradiation on the zero quantum (ZQ) or double quantum (DQ) transitions of electron-nuclear spin systems and results in negative and positive signal enhancements, respectively. (ii) The cross effect (CE) [7–9] describes the transfer of polarization from a pair of coupled electrons to their surrounding nuclei. When the Zeeman energies of the two electrons differ by about the nuclear Larmor frequency an on-resonance MW irradiation on one of the electrons can result in significant nuclear polarization enhancements. (iii) The term thermal mixing (TM) [10,11] has been used to describe systems with relatively high electron spin concentrations. The polarization transfer from the electrons to the nuclei in these systems has been previously described based on thermodynamic principles, taking into account the electron Zeeman, the nuclear Zeeman and the electron spin–spin energy reservoirs of the system.

The three mechanisms, SE, CE and TM, have been discussed extensively in the past and were described phenomenologically by rate equations describing the evolution of the nuclear spin magnetization of the bulk under continuous MW irradiation [11–14]. In a recent publication focused on the SE [15] we have proposed that additional insight into the DNP phenomena can be obtained by a quantum mechanical study of model microscopic spin systems. Based on density matrix simulations and taking into account different relaxation rates in the system, we demonstrated the important role electron spin relaxation (T_{1e}) plays in obtaining full polarization of the nuclear spins of the core. We also discussed the complexity of the SE in multi-nuclear environment. Recently, Köckenberger and co-workers performed numerical calculations showing the SE enhancement process in larger spin systems [16]. The purpose of this publication is to extend the quantum

* Corresponding author. Fax: +972 8 9344123.
E-mail address: yonatan.hovav@weizmann.ac.il (Y. Hovav).

1090-7807/$ - see front matter © 2011 Elsevier Inc. All rights reserved.
doi:10.1016/j.jmr.2011.09.047

mechanical approach to spin systems in which two electrons participate in the enhancement process, as in the CE case.

As is well known, the macroscopic enhancement measured in DNP requires both hyperfine couplings between electron spins with their neighbor (core) nuclear spins for direct transfer of polarization to these nuclei, as well as dipolar couplings between neighbor nuclear spins for transfer of polarization to the bulk nuclei. The basic mechanism of the polarization transfer to the bulk was discussed previously for SE-DNP [17]and will be extended in a separate publication taking into account CE-DNP processes.

The CE was first described by Kessenikh et al. [7,8] and further developed by Hwang and Hill [18,9]. Hwang and Hill measured the frequency dependence of the DNP enhancement on a polystyrene sample doped with a free radical. They showed that the positive and negative DNP enhancement peaks, which are separated by twice the nuclear Larmor frequency $2\omega_n$ in case of SE-DNP on samples with low radical concentrations, are shifting toward each other for increasing radical concentrations. To explain this phenomenon they used the theoretical framework described by Kessenikh et al. which takes into account two dipolar coupled electron spins in an inhomogeneous EPR line with spectral frequencies that are separated by the nuclear Larmor frequency $\pm\omega_n$. Under such conditions the allowed transition of one electron overlaps with the DQ or ZQ transition of the other electron. The coupling between the electrons can then cause an increase in the efficiency of the irradiation on the DQ or ZQ transitions. Phenomenological rate equations for the polarizations, derived on the basis of this concept, were then used to explain the shifts of the MW frequency positions at which the largest nuclear polarization enhancements were observed. The phenomenological description of the CE was further developed by Wollan [14] and Wind et al. [12]. More recently Griffin and coworkers [19,20], realizing the advantages of the CE, introduced the use of bi-radicals as DNP polarizing agents.

A quantum mechanical treatment of CE-DNP was very recently presented by Hu et al. [21,22], focusing on the polarization enhancement by bi-radicals. In the present work a similar treatment will be presented, while emphasizing the importance of electron and nuclear spin–lattice relaxation processes that result in high polarizations of the (core) nuclei surrounding dipolar coupled electron spin pairs.

In the following we first define the spin Hamiltonian of the spin systems under investigation and introduce the necessary relaxation parameters that are essential to the DNP induced nuclear polarization enhancement. After deriving the master equation of the elements of the spin density matrix in Liouville space, the SE- and CE-DNP mechanisms in a three-spin system, consisting of a coupled electron spin pair interacting with a single nucleus, are described. After introducing CE-DQ and CE-ZQ transitions and CE conditions, numerical results are presented demonstrating the unique properties of the spin dynamics during CE-DNP experiments. These calculations are followed by a careful analysis of the SE and CE processes in spin systems containing more than one nucleus. Here we restrict ourselves to non-interacting nuclear spins that resemble core nuclei. In the last section an effort is made to estimate the steady state polarization in a spin system including a pair of electrons surrounded by a multi-nuclear core. This discussion clearly demonstrates the complexity of the CE-DNP enhancement process.

2. Theoretical description

2.1. The spin interactions and spin relaxation

The theoretical framework for the following description of the DNP mechanism is similar to what has been used to describe the SE-DNP mechanism in our previous publication [15]. We will consider here a static spin system, composed of $N_e = 2$ unpaired electrons ($S = \frac{1}{2}$) and N_n nuclei ($I = \frac{1}{2}$), positioned in an external magnetic field pointing in the z-direction. In order not to complicate our derivations we will restrict ourselves to equivalent nuclei. We will thus refrain from discussing the influence on the DNP experiments of additional nuclei that are very strongly hyperfine coupled to the electrons, such as nitrogen in nitroxide radicals. The Hamiltonian of the system is composed of the hyperfine and dipolar interactions between the spins, and we assume that the system experiences a continuous MW irradiation at a frequency ω_{MW}. The form of the Hamiltonian describing this system in the MW rotating frame is given by [23]:

$$H = H_Z + H_{hfi} + H_D + H_d + H_{MW} = H_0 + H_{MW}, \tag{1}$$

where the different terms are:

$$\begin{aligned} H_Z &= \Delta\omega_a S_{z,a} + \Delta\omega_b S_{z,b} - \omega_n \sum_{i=1}^{N_n} I_{z,i} \\ H_{hfi} &= \sum_{\varepsilon=a,b;i=1,\ldots,N_n} A_{z,\varepsilon i} S_{z,\varepsilon} I_{z,i} + \frac{1}{2}\left(A^{+}_{\varepsilon i} S_{z,\varepsilon} I^{+}_{i} + A^{-}_{\varepsilon i} S_{z,\varepsilon} I^{-}_{i}\right) \\ H_D &= D_{ab}(3S_{z,a}S_{z,b} - \bar{S}_a.\bar{S}_b) \\ H_d &= \sum_{i<j} d_{ij}(3I_{z,i}I_{z,j} - \bar{I}_i.\bar{I}_j) \\ H_{MW} &= \omega_1(S_{x,a} + S_{x,b}), \end{aligned} \tag{2}$$

with a, b denoting the two electrons and $i, j = 1,\ldots,N_n$ the nuclei. The first term H_Z describes the Zeeman Hamiltonian in the rotating frame. The coefficients $\Delta\omega_a$ and $\Delta\omega_b$ determine the shift of the single electron transitions relative to the MW irradiation frequency ω_{MW}, including the frequency shift due to the g-tensor interaction of each electron. The nuclear Zeeman term is determined by the Larmor frequency ω_n of all nuclei, which for simplicity have the same chemical shift. The next terms H_{hfi}, H_D and H_d represent the spin–spin interactions including the truncated electron-nuclear hyperfine interaction, the electron–electron dipolar interactions, and the nuclear spin–spin dipolar interactions, respectively. All coefficients in these terms depend on the geometry of the spin system, i.e. on the magnitudes and directions of the inter-atomic distance vectors with respect to the external magnetic field. These terms are combined in the spin-interaction Hamiltonian H_0. The last term H_{MW} represents a MW field of intensity ω_1, applied in the x-direction. In the following sections we restrict ourselves to systems in which the nuclear dipole–dipole interactions are truncated by the hyperfine interactions, i.e. with $\|H_d\| \ll \|H_{hfi}\|$. Therefore in this publication we ignore the influence of H_d on the spin dynamics.

To describe the DNP spin dynamics and evaluate the nuclear polarizations we follow the theoretical approach introduced in Ref. [15]. At first H_0 is diagonalized:

$$\Lambda_0 = D^{-1} H_0 D. \tag{3}$$

This results in a set of 2^{N_n+2} eigenstates $|\lambda_k\rangle$ with eigenvalues λ_k. The MW Hamiltonian, H_{MW}, is then transferred to the same diagonalized frame

$$\Lambda_{MW} = D^{-1} H_{MW} D = \omega_1 D^{-1} S_x D$$

and contains (non-diagonal) matrix elements that can be considered as effective irradiation fields $\omega_{1,kk'}$ applied on the single transitions $|\lambda_k\rangle - |\lambda_{k'}\rangle$:

$$\omega_{1,kk'} = 2\langle\lambda_k|\Lambda_{MW}|\lambda_{k'}\rangle. \tag{4}$$

To evaluate the time evolution of the spin system we also apply the diagonalization transformation to the product state based density matrix

$$\rho^{\Lambda}(t) = D^{-1}\rho(t)D. \tag{5}$$

The populations of all $|\lambda_k\rangle$ states, defined by

$$p_k(t) = \langle\lambda_k|\rho^{\Lambda}(t)|\lambda_k\rangle, \tag{6}$$

are normalized such that $\sum_k p_k(t) = 1$. At thermal equilibrium the diagonal spin–density matrix ρ^{Λ}_{eq} has populations that are determined by the Boltzmann distribution:

$$\frac{p_{k'}(0)}{p_k(0)} = \varepsilon_{kk'} = \exp\{\hbar[(\lambda_k - \lambda_{k'}) + \omega_{MW}(M_{e,k} - M_{e,k'})]/k_BT\}, \tag{7}$$

where $M_{e,k''}$ is the total electron angular momentum component in the z direction of a state $|\lambda_{k''}\rangle$, which can be equal to ±1 or 0.

Spin–lattice and spin–spin relaxation mechanisms are introduced by defining effective relaxation rates $T^{-1}_{1,kk'}$ and $T^{-1}_{2,kk'}$ that drive the populations $p_k(t)$ and $p_{k'}(t)$ to their thermal equilibrium ratio, according to Eq. (7), and cause a decay of the $\langle\lambda_k|\rho^{\Lambda}(t)|\lambda_{k'}\rangle$ coherences, respectively. These rates are inserted into the spin density master equation in Liouville space in the same way as described in Ref. [15].

The values of the spin–lattice $T^{-1}_{1,kk'}$'s are derived from a set of the electron, nuclear and cross relaxation rates, $T^{-1}_{1,\varepsilon}, T^{-1}_{1,i}$ and $T^{-1}_{1,\varepsilon i}$ respectively. In Ref. [15] $T^{-1}_{1,kk'}$ rates for all transitions $|\lambda_k\rangle - |\lambda_{k'}\rangle$ were calculated by assuming that they depend on the values of the linear transition moments $m^{kk'}_{\varepsilon} = |\langle\lambda_k|2S_{x,\varepsilon}|\lambda_{k'}\rangle|^2$ and $m^{kk'}_{i} = |\langle\lambda_k|2D^{-1}I_{x,i}D|\lambda_{k'}\rangle|^2$. Here we extend these derivations by considering in addition the bilinear transition moments $m^{kk'}_{\varepsilon i} = |\langle\lambda_k|D^{-1}(S^+_{\varepsilon}I^+_i + S^+_{\varepsilon}I^-_i + S^-_{\varepsilon}I^+_i + S^-_{\varepsilon}I^-_i)D|\lambda_{k'}\rangle|^2$, representing the cross relaxation process originating from fluctuating hyperfine interaction terms. Combining the influence of all three type of moments we define the spin–lattice relaxation rates by

$$T^{-1}_{1,kk'} = \sum_{\varepsilon=1,2;i=1,N} m^{kk'}_{\varepsilon}T^{-1}_{1,\varepsilon} + m^{kk'}_{i}T^{-1}_{1,i} + m^{kk'}_{\varepsilon i}T^{-1}_{1,\varepsilon i}. \tag{8}$$

In all our derivations we assumed that $T^{-1}_{1,\varepsilon} \gg T^{-1}_{1,i}, T^{-1}_{1,\varepsilon i}$. In such a case the influence of the $T^{-1}_{1,\varepsilon i}$ rate on the spin dynamics is similar to that of $T^{-1}_{1,i}$ [15]. Electron–electron cross relaxation rates $T^{-1}_{1,ab}$ were not taken into account during our simulations. This is justified as long as $T^{-1}_{1,\varepsilon} \gg T^{-1}_{1,ab}$ and the combined action of $T^{-1}_{1,a}$ and $T^{-1}_{1,b}$ is more effective than $T^{-1}_{1,ab}$.

In the present simulations the $T^{-1}_{2,kk'}$ relaxation rates were simply introduced by choosing two fixed values for the decay of the electron and nuclear coherences, T^{-1}_{2e} and T^{-1}_{2n} respectively. To decide which of these two values must be assigned to each $T^{-1}_{2,kk'}$, we checked whether the $m^{kk'}_{\varepsilon}$ coefficients are different from zero $\left(T^{-1}_{2,kk'} = T^{-1}_{2e}\right)$ or equal to zero $\left(T^{-1}_{2,kk'} = T^{-1}_{2n}\right)$ [15].

After the diagonalization of H_0, each of the $|\lambda_k\rangle - |\lambda_{k'}\rangle$ eigenstate-transitions has off-resonance values $\Delta\omega_{kk'}$, defined by

$$\Delta\omega_{kk'} = (\lambda_k - \lambda_{k'}), \tag{9}$$

in addition to its parameters $\omega_{1,kk'}, T^{-1}_{1,kk'}$ and $T^{-1}_{2,kk'}$.

During the DNP experiments we are interested in following the magnitudes of the polarization of each nucleus i, defined by

$$P_i(t) = Tr\left(\rho^{\Lambda}(t)D^{-1}I_{z,i}D\right), \tag{10}$$

which about equals to $\sum_k p_k(t)[D^{-1}I_{zi}D]_{kk}$, with $[X]_{kk}$ the diagonal element of X in the $\{|\lambda_k\rangle\}$ representation. The success of the polarization transfer from the electrons to the nuclei can be evaluated by dividing $P_i(t)$ by the thermal equilibrium polarization of an electron, $P_a(0)$,

$$\begin{aligned}\pi_{e;i}(t) &= P_i(t)/P_a(0)\\ P_a(0) &= -Tr\left(\rho^{\Lambda}_{eq}D^{-1}S_{z,a}D\right).\end{aligned} \tag{11}$$

Our main interest lies in the spin dynamics of systems containing two electrons and many nuclei during MW irradiation. Using the interaction parameters of Eq. (2) and the relaxation rates of the system, the matrix elements of the Liouville superoperator can be constructed and the master equation for the elements of the density matrix can be solved. Its solution will enable us to derive the time dependences of $P_i(t)$. The numerical results obtained in this paper were calculated using a self-written MATLAB (MathWorks©) based computer program.

3. Two electrons and one nucleus

3.1. The Hamiltonian

We start by considering the Hamiltonian of a system consisting of a single nucleus n coupled to two electrons a and b, which is the simplest spin system experiencing the CE-DNP mechanism. The diagonal and off-diagonal elements of H_0 in the rotating frame of the MW irradiation field are dependent on the coefficients

$$\begin{aligned}\Sigma A_{z,n} &= A_{z,an} + A_{z,bn} \quad & \delta A_{z,n} &= A_{z,an} - A_{z,bn}\\ \Sigma A^+_n &= A^+_{an} + A^+_{bn} \quad & \delta A^+_n &= A^+_{an} - A^+_{bn}\\ \Sigma\omega_e &= \Delta\omega_a + \Delta\omega_b \quad & \delta\omega_e &= \Delta\omega_a - \Delta\omega_b\end{aligned} \tag{12}$$

as well as on D_{ab} and ω_n. In the product basis $|\chi_a;\chi'_b;\chi''_n\rangle$, with $\chi, \chi', \chi'' = \alpha, \beta$, H_0 has non-zero diagonal elements $E^{\chi''_n}_{\chi_a,\chi'_b}$ (the subscripts define the electron states and the superscript the nuclear state)

$$\begin{aligned}E^{\alpha_n/\beta_n}_{\beta_a\beta_b} &= \frac{1}{2}\left(-\Sigma\omega_e + D_{ab} \mp \omega_n \mp \frac{1}{2}\Sigma A_{z,n}\right)\\ E^{\alpha_n/\beta_n}_{\alpha_a\beta_b} &= \frac{1}{2}\left(\delta\omega_e - D_{ab} \mp \omega_n \pm \frac{1}{2}\delta A_{z,n}\right)\\ E^{\alpha_n/\beta_n}_{\beta_a\alpha_b} &= \frac{1}{2}\left(-\delta\omega_e - D_{ab} \mp \omega_n \mp \frac{1}{2}\delta A_{z,n}\right)\\ E^{\alpha_n/\beta_n}_{\alpha_a\alpha_b} &= \frac{1}{2}\left(\Sigma\omega_e + D_{ab} \mp \omega_n \pm \frac{1}{2}\Sigma A_{z,n}\right),\end{aligned} \tag{13}$$

and the off-diagonal elements

$$\begin{aligned}&\langle\alpha_a,\alpha_b;\alpha_n|H_0|\alpha_a,\alpha_b;\beta_n\rangle = -\langle\beta_a,\beta_b;\alpha_n|H_0|\beta_a,\beta_b;\beta_n\rangle = \frac{1}{4}\Sigma A^+\\ &\langle\alpha_{e1},\beta_b;\alpha_n|H_0|\alpha_a,\beta_b;\beta_n\rangle = -\langle\beta_a,\alpha_b;\alpha_n|H_0|\beta_a,\alpha_b;\beta_n\rangle = \frac{1}{4}\delta A^+\\ &\langle\alpha_a,\beta_b;\alpha_n/\beta_n|H_0|\beta_a,\alpha_b;\alpha_n/\beta_n\rangle = -\frac{1}{2}D_{ab}.\end{aligned} \tag{14}$$

The energy level diagram corresponding to the Zeeman interaction of this system is shown in Fig. 1a.

As long as the hyperfine and dipolar coefficients are much smaller than the nuclear Zeeman frequency, most of the differences between the energies are larger than their corresponding off diagonal elements. Perturbation theory can then be exploited to express the influence of these off-diagonal elements on the eigenstates of the system (for a full diagonalization see Ref. [21]). This mixing of the product states will be denoted by assigning the states by an *-sign. In the SE-DNP case the pseudo-secular hyperfine elements cause very weak mixing between the product spin states, resulting in finite values for the effective MW fields $\omega_{1,kk'}$ on the DQ and ZQ transitions. This is shown schematically in Fig. 1c.

The off-diagonal elements of H_0 can have a large impact on the spin dynamics when pairs of energies become degenerate. One such case occurs when two electrons have about the same Larmor frequency, $|\delta\omega_e| \ll |\frac{1}{2}D_{ab}|$, and a flip-flop of the electronic spin states does not influence by much the total energy of the system: $E^{\alpha_n/\beta_n}_{\alpha_a\beta_b} \approx E^{\alpha_n/\beta_n}_{\beta_a\alpha_b}$. Then, the electron–electron flip-flop term of H_D becomes very significant for the spin dynamics (as long as $|D_{ab}| \gg |\delta A_z|$) [23]. Even when $|\delta\omega_e| \gg |\frac{1}{2}D_{ab}|$, the dipolar interaction causes a mixing between electronic states that in turn creates an indirect interaction between electron b and the nucleus, even

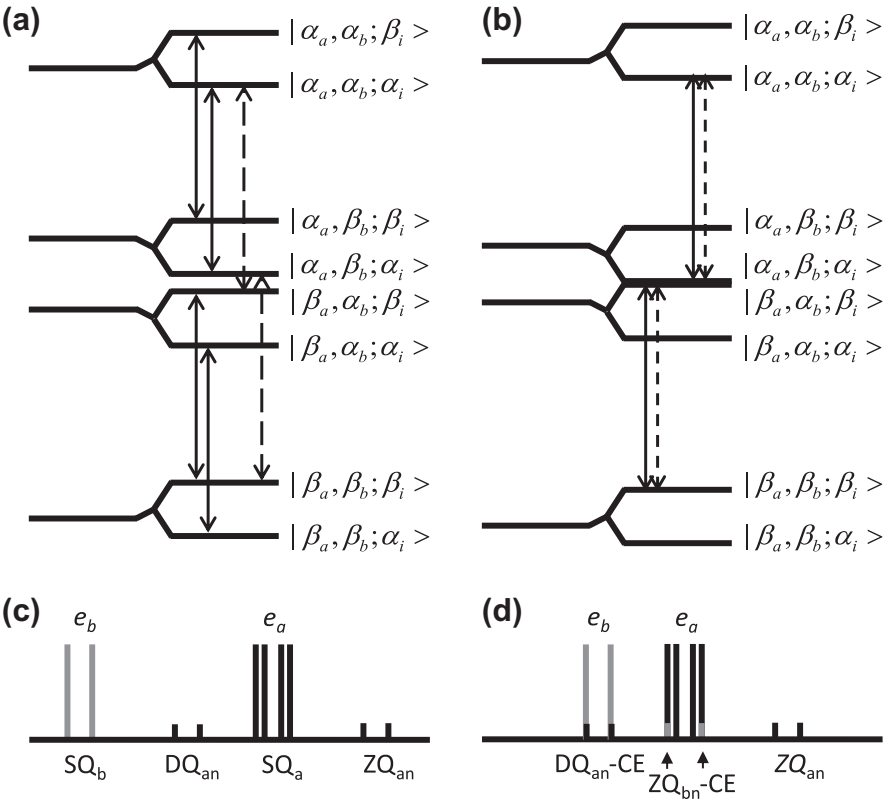

Fig. 1. Schematic energy level diagrams of a $\{e_b - e_a - n\}$ spin system, in an arbitrary MW rotating frame, (a) removed from any CE condition and (b) at the CE condition $\delta\omega_e = \omega_n$. In (a) the four SQ_b (solid arrows) and two DQ_{an} (dashed arrows) transitions are indicated, and in (b) the two SQ_b and two DQ_{an} forming the DQ_{an}–CE transitions. Schematic (stick diagram) EPR spectra of the system are shown in (c) and (d), corresponding to (a) and (b), respectively. For simplicity the hyperfine interaction between the nucleus and electron b was set to zero. The SQ_a transition is split into four lines, due to the electron dipolar and hyperfine interactions, while the DQ_{an}, ZQ_{an}, and SQ_b transitions are split into two, due to the electron dipolar interaction. The SQ_b and ZQ_{bn}-CE transitions are shown in gray. The DQ_{bn} and ZQ_{bn} SE transitions are not indicated for simplicity.

when $A_{bn}^{\pm} = 0$. This electron state mixing will also be marked by an *-sign.

A degeneracy relevant for DNP occurs when the difference $\delta\omega_e$ between the Larmor frequencies of the electrons equals to the nuclear Zeeman frequency,

$$\delta\omega_e \cong \pm\omega_n, \tag{15}$$

and degeneracies of the following form are encountered:

$$E^{\alpha_n}_{\alpha_a\beta_b} \cong E^{\beta_n}_{\beta_a\alpha_b} \quad \text{or} \quad E^{\beta_n}_{\alpha_a\beta_b} \cong E^{\alpha_n}_{\beta_a\alpha_b}. \tag{16}$$

We will refer to these degeneracies as the CE conditions. The Zeeman energy level diagram of this system for $E^{\alpha_n}_{\alpha_a\beta_b} \cong E^{\beta_n}_{\beta_a\alpha_b}$ is schematically drawn in Fig. 1b.

To evaluate the form of the degenerate eigenstates at these conditions we can use degenerate perturbation theory [24], realizing that the degenerate states are (indirectly) connected via the non-zero matrix elements $\langle\alpha_a, \beta_b; \alpha_n|H_0|\alpha_a, \beta_b; \beta_n\rangle = \delta A^+$ and $\langle\alpha_a, \beta_b; \beta_n|H_0|\beta_a, \alpha_b; \beta_n\rangle = D_{ab}$. At the DQ-CE condition $\delta\omega_e \simeq +\omega_n$ strong state mixing can occur, and the mixed eigenstates become [25,26]

$$\begin{aligned} |(\alpha_a, \beta_b; \alpha_n)^*\rangle &= \cos\varphi_{CE}|\alpha_a, \beta_b; \alpha_n\rangle + \sin\varphi_{CE}|\beta_a, \alpha_b; \beta_n\rangle \\ |(\beta_a, \alpha_b; \beta_n)^*\rangle &= \cos\varphi_{CE}|\beta_a, \alpha_b; \beta_n\rangle - \sin\varphi_{CE}|\alpha_a, \beta_b; \alpha_n\rangle \\ \tan 2\varphi_{CE} &\simeq \frac{1}{2}\frac{\delta A^+}{\omega_n}\frac{D_{ij}}{(\delta\omega_e - \omega_n)}. \end{aligned} \tag{17}$$

Similar equations can be derived for the ZQ-CE condition $\delta\omega_e \simeq -\omega_n$. This results in maximal state mixing for $\varphi_{CE} = \pi/4$, while this mixing decays fast to zero when $\delta\omega_e$ deviates from $\pm\omega_n$. The degenerate state mixing is the basis of the difference between the SE-DNP and CE-DNP process and is therefore essential for all further discussions.

At the CE conditions the DQ_{an} or ZQ_{an} transitions of nucleus n interacting with electron a overlap with a single quantum transition of electron b (SQ_b). The overlapping transitions are denoted as DQ_{an}–CE and ZQ_{an}–CE transitions. This is schematically shown in Fig. 1d.

3.2. The effective MW fields and electronic relaxation

In the diagonalized representation the MW Hamiltonian Λ_{MW} is composed of elements that can be described as single transition effective irradiation fields $\omega_{1kk'}$. Away from the CE conditions, the $DQ_{\varepsilon n}$ and $ZQ_{\varepsilon n}$ DNP transitions experience weak effective fields of magnitudes $s_{SE}\omega_1$, with s_{SE} equal to $\delta A^+/2\omega_n$ or $\Sigma A^+/2\omega_n$, depending on the corresponding states of the electrons. At the CE conditions the effective fields of the $DQ_{\varepsilon n}$-CE and $ZQ_{\varepsilon n}$-CE transitions, $s_{CE}\omega_1$, can become as large as $\omega_1/\sqrt{2}$. For example, the effective MW fields of the two DQ_{an}–CE and the two ZQ_{bn}–CE transitions (see Fig. 1d), when $\delta\omega_e \approx \omega_n$, become

$$\begin{aligned} &\left\langle \alpha_a, \alpha_b, \alpha_n^*|\omega_1 D^{-1} S_x D|(\beta_a, \alpha_b; \beta_n)^*\right\rangle = \left\langle (\alpha_a, \beta_b, \alpha_n)^*|\omega_1 D^{-1} S_x D|\beta_a, \beta_b; \beta_n^*\right\rangle \\ &= \omega_1 \sin\varphi_{CE} \\ &\left\langle \alpha_a, \alpha_b, \beta_n^*|\omega_1 D^{-1} S_x D|(\alpha_a, \beta_b, \alpha_n)^*\right\rangle = \left\langle (\beta_a, \alpha_b; \beta_n)^*|\omega_1 D^{-1} S_x D|\beta_a, \beta_b; \alpha_n^*\right\rangle \\ &= \omega_1 \sin\varphi_{CE} \end{aligned} \tag{18}$$

where $\varphi_{CE} = \pi/4$. Each of these $\omega_{1,kk'}/2$ off diagonal elements of Λ_{MW}, connecting $|\lambda_k\rangle$ with $|\lambda_{k'}\rangle$ states, has its own off resonance

value $\Delta\omega_{kk'}$ (see Eq. (9)). For example, in order to apply an on-resonance MW field at one of the frequencies of the two DQ_{an}-CE transitions, the MW frequency must be close to $\omega_{MW} = \omega_b \pm (D_{ab} + A_{z,bn})$.

The relaxation rates in the diagonalized frame are also influenced by the degeneracy. For example, at the CE condition the cross relaxation rates $T^{-1}_{1,DQ/ZQ}$ of the DQ_{an} and ZQ_{bn} transitions becomes of the same order of magnitude as the electron $T^{-1}_{1,\varepsilon}$ rates. In practice this can become significant when cross-relaxation rates induced by the hyperfine interaction are smaller than $T^{-1}_{1,\varepsilon}$. These relaxation rates can reduce the off-resonance excitation profile of the DQ–CE transitions, as will be explained in what follows.

3.3. Ideal DNP experiments

The polarization enhancement during an ideal SE-DNP experiment was discussed in Refs. [15,17] for a two-spin system $e_a - n$. There it was shown that when saturating the DQ_{an} or ZQ_{an} transition, with $(s_{SE}\omega_1)^2 T_{1DQ/ZQ} T_{2DQ/ZQ} \gg 1$ and $T^{-1}_{1a} \gg T^{-1}_{1DQ/ZQ}$, the SE mechanism can result in a steady state polarization $P_n(t) = \pm P_e(t) = \pm P_e(0)$, respectively. In our three-spin system, containing two electrons and one nucleus, $\{e_b - e_a - n\}$, the SE-DNP mechanism can also induce nuclear polarization as long as the CE condition is not fulfilled. In this system the DQ_{an} and ZQ_{an} transitions are split by the dipolar coefficient D_{ab} (Fig. 1c). In the ideal case, when we succeed to saturate both DQ_{an} transitions simultaneously by a MW irradiation and when $T^{-1}_{1,a} \gg T^{-1}_{1n}$, the following relations between the populations will be reached after some time:

$$\begin{aligned} p(\alpha^*_a, \beta^*_b; \beta^*_n; t) &= \varepsilon_e p(\beta_a, \beta_b; \beta^*_n; t) = \varepsilon_e p(\alpha^*_a, \beta^*_b; \alpha^*_n; t) \\ &= \varepsilon_e^2 p(\beta_a, \beta_b; \alpha^*_n; t) \end{aligned} \tag{19}$$

and

$$\begin{aligned} p(\alpha_a, \alpha_b; \beta^*_n; t) &= \varepsilon_e p(\beta^*_a, \alpha^*_b; \beta^*_n; t) = \varepsilon_e p(\alpha_a, \alpha_b; \alpha^*_n; t) \\ &= \varepsilon_e^2 p(\beta^*_a, \alpha^*_b; \alpha^*_n; t), \end{aligned} \tag{20}$$

where $\varepsilon_e = \exp\{-\hbar\omega_e/k_B T\}$ is the Boltzmann factor for the electrons. In addition the $T^{-1}_{1,b}$ rate will maintain the condition

$$p(\chi_a, \beta_b; \chi^*_n; t) = \varepsilon_e p(\chi_a, \alpha_b; \chi^*_n; t). \tag{21}$$

A straightforward check shows then that the total nuclear polarization becomes $P_n(t) = P_e(0)$. The same type of calculation for the ZQ_{an} transitions will result in $P_n(t) = -P_e(0)$.

When we are dealing with bi-radicals we can expect their electron dipolar interactions to be large, and for most of their orientations it will not be possible to saturate both DQ_{an} or ZQ_{an} dipolar satellites by a single MW irradiation. In such an event the effect of the irradiation, together with $T^{-1}_{1,a}$, will result either in Eq. (19) or Eq. (20). However, $T^{-1}_{1,b}$ will cause the steady state populations to satisfy both equations, resulting again in polarizations of the form $P_i(t) = \pm P_e(0)$. This is in contrast to the effect of the splitting of the DQ_{an} and ZQ_{an} transitions due to the presence of additional core nuclei, which reduces the end polarizations [15].

When $\delta\omega_e \cong \pm\omega_n$ and a MW field is applied on one of the DQ_{an}-, ZQ_{bn}-, or ZQ_{an}-, DQ_{bn}-CE dipolar satellites, the CE-DNP mechanism is the source of the enhancement. For example, when both of the dipolar split DQ_{an} transitions and the four SQ_{bn} transitions are saturated by a single MW field, we get three sets of equal populations:

$$\begin{aligned} &p(a_a, \alpha_b; \beta^*_n; t) = p(a^*_a, \beta^*_b; \beta^*_n; t) \\ &p(a_a, \alpha_b; \alpha^*_n; t) = p((a_a, \beta_b; \alpha_n)^*; t) = p((\beta_a, \alpha_b; \beta_n)^*; t) \\ &\quad = p(\beta_a, \beta_b; \beta^*_n; t) \\ &p(\beta^*_a, \alpha^*_b; \alpha^*_n; t) = p(\beta_a, \beta_b; \alpha^*_n; t). \end{aligned} \tag{22}$$

These populations will be separated by the action of $T^{-1}_{1,a}$ and will result again in $P_n(t) = +P_a(0)$. When the MW irradiation saturates only one of the dipolar split DQ_{an}–CE transitions and two of the SQ_{bn} transitions, two groups of equal populations are obtained:

$$\begin{aligned} &p((a_a, \beta_b; \alpha_n)^*; t) = p((\beta_a, \alpha_b; \beta_n)^*; t) = p(\beta_a, \beta_b; \beta^*_n; t) \\ &p(\beta^*_a, \alpha^*_b; \alpha^*_n; t) = p(\beta_a, \beta_b; \alpha^*_n; t). \end{aligned} \tag{23}$$

The effect of the electron $T^{-1}_{1,a}$ and $T^{-1}_{1,b}$ spin lattice relaxation rates is not as simple as before. The end population $P_n(t)$ in this case depends on the relative values of the relaxation rates of the two electrons, and can vary between $P_e(0)$ (for $T^{-1}_{1,a} \gg T^{-1}_{1,b}$) and values smaller than $0.5P_e(0)$ (for $T^{-1}_{1,a} \ll T^{-1}_{1,b}$). A numerical example of this will be shown in the next section. Other irradiation schemes, such as a MW field on only one of the SQ_b transitions, could also have been considered.

This discussion shows that the DNP enhancement depends on the ability to saturate the $DQ_{\varepsilon n}$ or $ZQ_{\varepsilon n}$ transitions in the system, combined with the effect of $T^{-1}_{1,a}$ and $T^{-1}_{1,b}$. As a result large polarizations can be reached even when only parts of these transitions are saturated.

The on-resonance saturation level of the different transitions $|\lambda_k\rangle - |\lambda_{k'}\rangle$ depends on the values of $\left\{\omega^2_{1kk'} T_{1,kk'} T_{2,kk'}\right\}$ and possible combinations of spin lattice relaxation pathways in the system that can replace $T^{-1}_{1,kk'}$ [15]. The width of the off-resonance MW excitation profile of a transition can be characterized by the off resonance value $\Delta\omega_{1/2,kk'}$ at which the steady state population difference $p_k(t) - p_{k'}(t)$ reaches a value that is half of the difference at thermal equilibrium. When the effective MW field is strong enough to saturate a transition on resonance, with the saturation condition $\omega^2_{1kk'} T_{1,kk'} T_{2,kk'} \gg 1$, this width is given by $\Delta\omega_{1/2,kk'} \approx \omega_{1kk'} \sqrt{T_{1,kk'}/T_{2,kk'}}$. In the case of the SE this is given by $\Delta\omega_{1/2,SE} \approx s_{SE}\omega_1 \sqrt{T_{1,DQ/ZQ}/T_{2,e}}$ for DQ or ZQ irradiation, with $T_{1DQ/ZQ}$ in the order of T_{1n} and $T_{1,\varepsilon n}$. At the ideal CE condition we get $\Delta\omega_{1/2,SE} \approx \frac{1}{\sqrt{2}}\omega_1 \sqrt{2T_{1,e}/T_{2,e}}$. As will be also shown numerically in the next section, the CE-DNP mechanism can have a significantly broader excitation bandwidth relative to the SE-DNP mechanism. The first can therefore be much more efficient. Additionally, the increase in the effective MW irradiation strength of CE-DNP is expected to play a significant role during the DNP-assisted spin diffusion process polarizing the bulk.

The (not necessarily exponential) rise time of the nuclear polarization in the SE case (neglecting off resonance irradiation of SQ transitions) was shown [15] to be limited by $T_{1,\varepsilon} \lesssim \tau_{DNP} \lesssim T_{1,DQ/ZQ}, T_{1,n}$. In the case of CE-DNP $T_{1,DQ/ZQ} \approx 2T_{1,\varepsilon}$ and the value of τ_{DNP} will be in the order of $T_{1,\varepsilon}$.

In the next section frequency profiles of the steady state polarizations, obtained by solving the spin density operator numerically, together with nuclear polarization build up curves of a $\{e_b - e_a - n\}$ spin system are shown.

3.4. Numerical simulations

The interaction and relaxation parameters of the three-spin system under consideration with two electrons and one proton $\{e_b - e_a - n\}$, are summarized in Table 1. To simplify the interpretation of the numerical results we have chosen a system in which the nucleus is positioned closer to electron a than to electron b, resulting in $|A_{z,bn}| \ll |A_{z,an}|$, and $|A^{\pm}_{bn}| \ll |A^{\pm}_{an}|$. The electron dipolar interaction strength was chosen to correspond to an electron–electron distance of 12.8 Å, as in TOTAPOL radicals [20]. The interaction and relaxation parameters are similar to values found in DNP experiments. The MW power was chosen such that irradiated transitions can reach saturation when irradiated on resonance.

Fig. 2 shows the nuclear steady state polarization as a function of the MW frequency ω_{MW}, for different values of $\delta\omega_e = \omega_a - \omega_b$. In

Table 1
The interaction and relaxation parameters used during the simulations for a $\{e_b - e_a - n\}$ spin system. All other parameters, and modifications of the values given here, are given in the figure captions. The interactions were calculated for an electron b positioned at a distance 12.8 Å away from electron a in the x direction, and a distance vector $\bar{r}_{an}$ connecting nucleus n with electron a with $|\bar{r}_{an}| = 4.41$ Å and making an angle of 45^0 with the z−axis. A temperature of 10 K was used in all relevant simulations.

Parameter	Value
$D_{ab}/2\pi$	−12.46 MHz
$A_{z,an}/2\pi$	−0.46 MHz
$A_{z,bn}/2\pi$	0.02 MHz
$A^{+}_{an}/2\pi$	1.38 MHz
$A^{+}_{bn}/2\pi$	0.01 MHz
$\omega_n/2\pi$	144 MHz*
$\omega_1/2\pi$	0.1 MHz
$T_{1,a/b}$	10 ms
$T_{1,an}$	2.5 s
$T_{1,bn}$	1000 s**
$T_{1,n}$	10 s**
T_{2e}	10 μs
T_{2n}	1 ms

* Simulations were performed for ^1H nuclei.
** Unless stated otherwise, this value was used for all nuclei in the spin systems.

all cases we keep ω_a fixed and change the value of ω_b, for simplicity. When $\delta\omega_e > \omega_n$ (in (a)) the nuclear polarization is determined mainly by the SE-DNP mechanism of electron a. The electron dipolar splitting does not cause any reduction of the maximal polarization, which reaches a value of $|P_n(t)| \simeq P_e(0)$, as in an $\{e_a - n\}$ system. In addition some hyper-polarization is obtained when irradiating the DQ_{bn} or ZQ_{bn} transitions of electron b. This originates from a small state mixing due to a combination of the dipolar interaction between a and b and the hyperfine interaction between a and n.

Next, the nuclear polarization is calculated at the CE condition $\delta\omega_e = \omega_n + \delta_{CE}$ (in (b)), where δ_{CE} represents some higher order correction to the degeneracy condition, and is in this example about equal to $\delta_{CE} \approx D^2_{ab}/2\omega_n$. The simulated $P_n(t)$ shows a polarization profile that is much broader around ω_a and ω_b than for the pure SE case. For the MW irradiation at each of the dipolar DQ_{an}–CE satellite transitions the end polarization reaches a value of about $|P_n(t)| \approx 0.7P_e(0)$. When the resonance frequencies of the two electrons are about equal, $|\delta\omega_e| < |D_{ab}|$, (in (c)) the dipolar state mixing increases the effective MW field on the DQ_{bn} and ZQ_{bn} transitions and shifts the energies of the system. The polarization profile for the system at its second CE condition (black line in (d)), when $\delta\omega_e = -\omega_n - \delta_{CE}$ is also shown. The order of the signs of the enhancements for increasing ω_{MW} is the same as in the first CE case, and follows the order for SE-DNP of each electron.

So far we assumed that the two electrons have the same spin–lattice relaxation rate. We next consider a 10-fold increase in the relaxation time of electron a, as given by the gray line in Fig. 2d. When the SQ_a transition is affected by the irradiation, this results in an increase of the enhancement width and an increase in the maximal polarization. The former is due to broader MW excitation width and the latter due to an increase in the $T_{1,a}/T_{1,b}$ ratio, as was previously explained. When the SQ_b transition is irradiated, the enhancement width remains the same, but the maximal enhancement decreases. Similar results can be obtained for a 10-fold increase in $T_{1,b}$.

To show the gradual transfer from CE- to SE-DNP enhancement in the same spin system, we consider a three-spin system close to the CE condition $\delta\omega_e = \omega_n + \delta_{CE}$. In Fig. 3a a contour of the steady state nuclear polarization is plotted as a function of the MW irradiation frequency around $\omega_{MW} = \omega_a - \omega_n + |D_{ab}|$ (x-axis), and of $\delta\omega_e$ (y-axis) for a fixed ω_a value. A close-up of the contour around the CE condition is shown in Fig. 3b. We observe again the broad MW frequency dependence of the enhancement at the CE condition (marked by an arrow), resulting from the high effective MW field. Note that the polarization profile as a function of $\delta\omega_e$ is rather narrow. Furthermore, it is interesting to notice that when moving away from the CE condition the enhancement varies as a function of $\delta\omega_e$, reaching values close to zero or even larger than one. Here we will not consider these localized polarization variations any further.

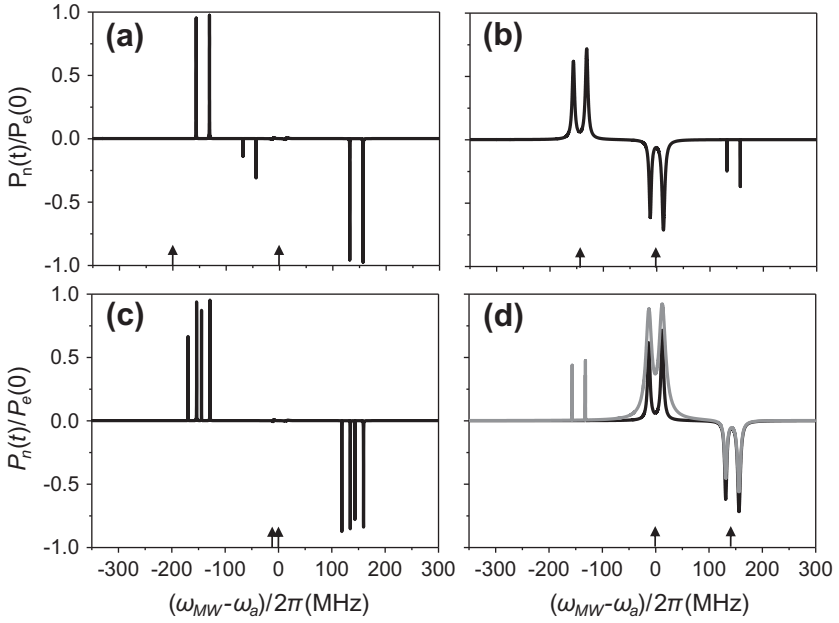

Fig. 2. The calculated steady state nuclear polarization of a $\{e_b - e_a - n\}$ spin system as a function the MW irradiation frequency. The value of ω_b was set at different values with respect to ω_a such that in (a) $\delta\omega_e/2\pi = 200$ MHz, in (b) $\delta\omega_e/2\pi = (\omega_n + \delta_{CE})/2\pi \simeq 143.46$ MHz, in (c) $\delta\omega_e/2\pi = 10$ MHz, and in (d) $\delta\omega_e/2\pi = -(\omega_n + \delta_{CE})/2\pi \simeq -143.46$ MHz. The position of the $\omega_a/2\pi$ and $\omega_b/2\pi$ frequencies are marked by arrows. The values of the interaction and relaxation parameters are given in Table 1. In (d) the calculation is repeated after increasing $T_{1,a}$ by a factor of ten (gray line).

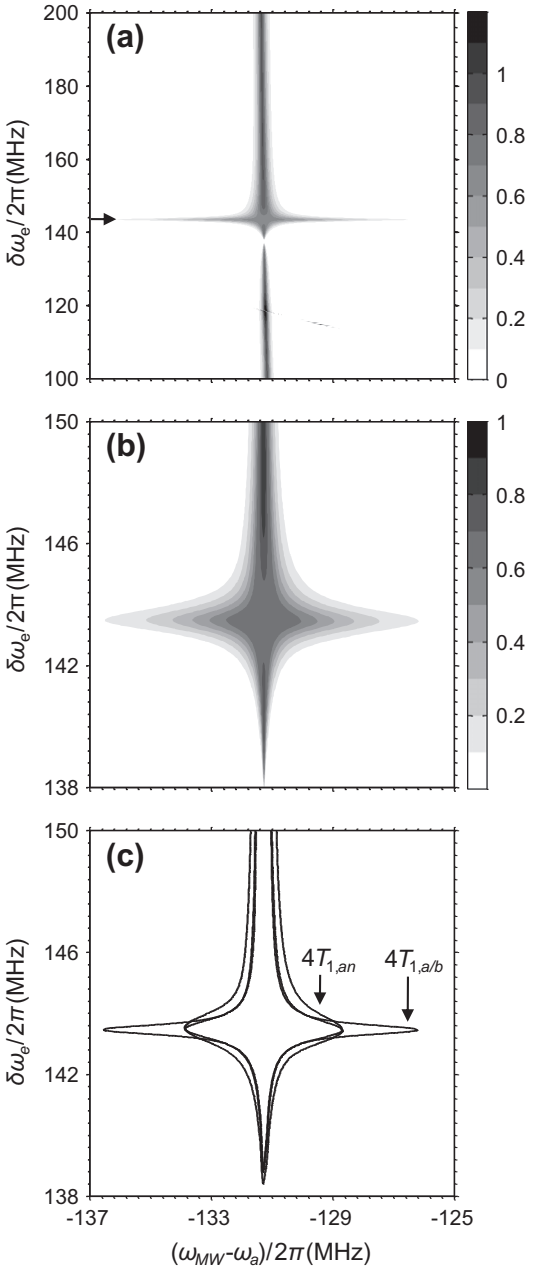

Fig. 3. In (a) a 2D map showing the calculated steady state nuclear polarization of a $\{e_b - e_a - n\}$ spin system as a function of the MW irradiation frequency, ω_{MW}, and of the difference between the EPR transition frequencies of the 2 electrons, $\delta\omega_e$. A selected area of this contour is repeated in (b). In (c) only the contour line of $P_n(t) = 0.4P_e(0)$ is drawn for the relaxation parameters used in (a) and (b), as well as for a four fold increase of $T_{1,a}$ and $T_{1,a}$, or of $T_{1,an}$. In all cases the MW irradiation was performed around $\omega_{MW} \simeq \omega_a - \omega_n - D_{ab}$, and around $\delta\omega_e = \omega_n$. All other interaction and relaxation parameters are given in Table 1.

The contours of constant polarization around the CE condition are strongly dependent on the electron and cross relaxation values, $T_{1,\varepsilon}$ and $T_{1,\varepsilon n}$. This is demonstrated in Fig. 3c, where the $P_n(t) = 0.4P_e(0)$ contour lines are drawn. An increase of $T_{1,\varepsilon}$ broadens the area of CE-DNP polarization in the ω_{MW} direction and keeps the width as a function of $\delta\omega_e$ constant, while an increase in $T_{1,an}$ results in an opposite effect. A change in $T_{1,n}$ broadens the contour line in a similar manner as observed for $T_{1,an}$.

The effect of the MW irradiation strength on the nuclear steady state polarization at the $\delta\omega_e = \omega_n + \delta_{CE}$ CE condition is shown in Fig. 4. When $\omega_1/2\pi = 0.1$ MHz (solid black line) the MW irradiation

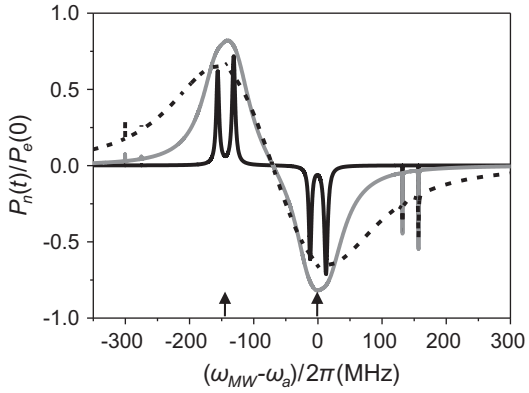

Fig. 4. The dependence of the steady state nuclear polarization of a $\{e_b - e_a - n\}$ spin system at its CE condition $\delta\omega_e/2\pi = (\omega_n + \delta_{CE})/2\pi \simeq 143.46$ MHz on the MW irradiation intensity. This intensity was set at $\omega_1/2\pi = 0.1$ MHz (solid black line), 1 MHz (solid gray line) and 3 MHz (dashed black line). All other interaction and relaxation parameters are given in Table 1.

is not sufficient to excite simultaneously the two dipolar DQ/ZQ satellites of the electrons. Increasing the MW intensity to 1 MHz (gray line) the off-resonance profiles of the polarization broadens and the maximal enhancements reach about the values ±1. Increasing the MW strength even more, $\omega_1 = 3$ MHz (dashed line), results in a lowering of the maximal enhancements due to on- and off-resonance irradiation of all EPR transitions. Here we considered SQ MW irradiation fields that are stronger than the hyperfine interactions, and did not address complications arising when this is not the case [22].

Typical temporal evolutions of the nuclear polarization during on and off-resonance MW irradiation of the DQ_{an} transitions are shown in Fig. 5 for a system at and away from the CE condition (note the difference in the time scales in the two figures). The rise-time τ_{DNP} of the nuclear polarization for the CE case (Fig. 5a) for on- and off-resonance irradiation are similar and in the order of $T_{1,DQ/ZQ}$, which can become equal to the upper limit $2T_{1\varepsilon}$ as discussed previously. The large effective MW field saturates the irradiated transition at an even faster time scale, as shown in the insert. This large field also results in a broad enhancement bandwidth as can be seen from the off-resonance dependence of the curves. Fig. 5b shows typical SE type of time evolutions, for a system in which the CE condition is not fulfilled. These curves demonstrate the slowing down of the rise time, reaching its limiting values, $T_{1,n}$, $T_{1,DQ/ZQ}$ when moving off-resonance. In this case the off-resonance polarization bandwidth becomes again narrow. For completeness, the time evolution of the populations in the on-resonance cases are shown in Fig. 5c and d.

4. Two electrons and many (core) nuclei

In this section we examine the DNP mechanism in systems containing two electrons and a multiple number of core nuclei. These systems are relevant for example when considering the spin dynamics of DNP on glassy solid solutions containing a low concentration of bi-radicals. The numerical results for the polarizations of the nuclei, using the master equation of the density operator in Liouville space, are evaluated for systems of up to 5-spins. Because the effective MW fields can become large in the CE case, we did not use the Hilbert space calculations as we did before in Ref. [17]. We note however, that while these calculations are not strictly valid in our case, they could have given rather accurate results for certain sets of interaction and relaxation parameters.

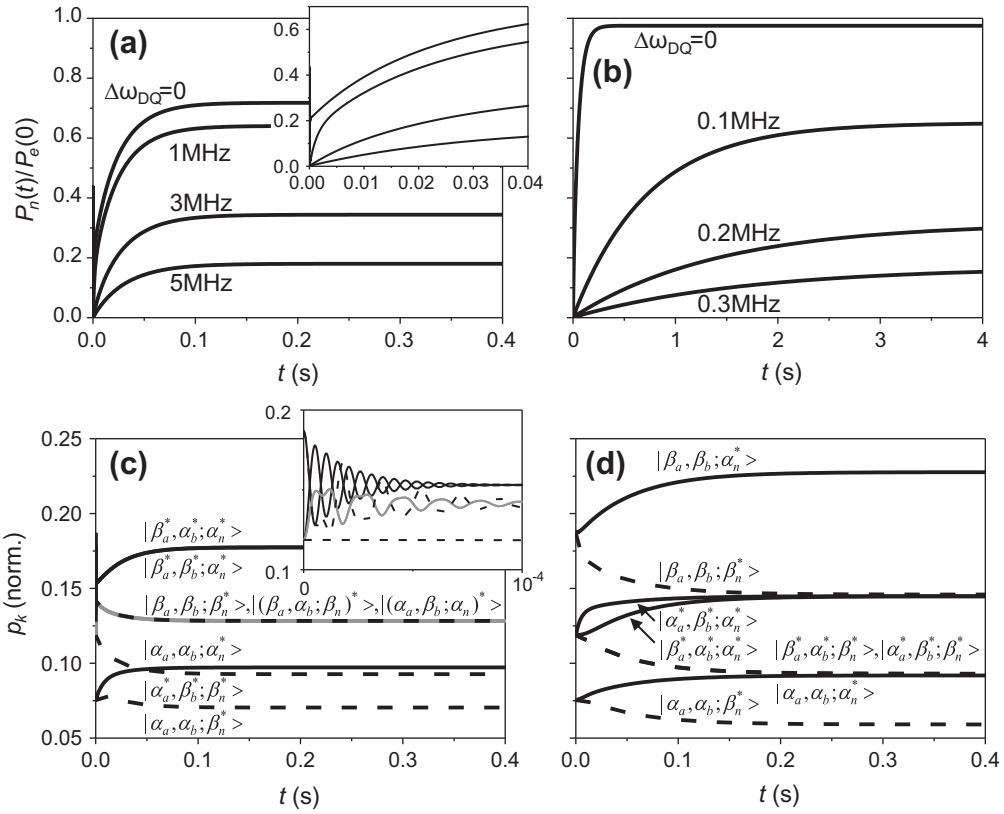

Fig. 5. The time evolutions of the nuclear polarization $P_n(t)$ and the populations $p_k(t)$ of the eigenstates of a $\{e_b - e_a - n\}$ spin system during a cw MW irradiation. In (a) and (c) the system is at the CE condition $\delta\omega_e/2\pi = (\omega_n + \delta_{CE})/2\pi \simeq 143.46$ MHz and in (b) and (d) at a SE condition with $\delta\omega_e/2\pi = 200$ MHz. The MW frequency is equal to that of the DQ_{an} transition around $\omega_{MW} \simeq \omega_a - \omega_n - D_{ab}$. In (a) and (b) the time dependence of $P_n(t)$ is also shown for different MW frequencies, as indicated in the figure. The inserts in (a) and (c) show the initial time dependences of $P_n(t)$ and $p_k(t)$. The CE mixed $|(\alpha_a, \beta_b; \alpha_n)^*\rangle$ and $|(\beta_a, \alpha_b; \beta_n)^*\rangle$ states are drawn in gray in (c). All interaction and relaxation parameters are given in Table 1.

4.1. The core and bulk nuclei

Before considering the DNP enhancement of multi-nuclear core systems surrounding a single electron pair, it is necessary to define the core. We realize that the actual nuclear signals we measure in experiments originate mainly from the bulk nuclei in the sample. Thus a description of the DNP mechanism must take into account the polarization transfer from the electrons to the directly hyperfine coupled core nuclei, and to the bulk nuclei by the nuclear dipole–dipole interaction. These processes are both driven by MW irradiation and electron spin relaxation . A possible distinction between the core and bulk nuclei has been discussed in our previous publications [17,15] and depends on the relative strength of the H_{hfi} terms with respect to the nuclear dipole–dipole interaction terms of H_d, since the first can truncate the off diagonal flip-flop terms of the second. For the SE case we previously defined a somewhat arbitrary boundary condition distinguishing between the core and bulk nuclei. The core nuclei were chosen as those that have hyperfine coupling constants that are larger than their dipolar flip-flop matrix elements with neighboring nuclei.

In systems based on interacting electrons in mono-radical solutions or on bi-radical solutions, the core nuclei interact with two electrons. We then define a nucleus i to belong to the core according to the condition

$$\zeta|d_{ij}|/2 < \sum_{\varepsilon=a,b} \frac{1}{2}|(A_{z,\varepsilon i} - A_{z,\varepsilon j})| + \frac{|A_{\varepsilon 1}^{\pm}|^2 - |A_{\varepsilon 2}^{\pm}|^2}{8|\omega_n|} \tag{24}$$

for all its close neighboring nuclei j. The core region in the case of a cubic nuclear lattice surrounding two coupled electrons, choosing $\zeta = 5$, is shown in Fig. 6. All other relevant interaction parameters used to generate the shape of the core are summarized in the figure caption. According to this somewhat arbitrary definition, the polarization inside the core is mainly driven directly by the electron-nuclear interactions, while the bulk polarization enhancement is assisted by the core-bulk and bulk-bulk dipolar interactions. However we should realize that for strong enough MW irradiation even the remaining dipolar interaction may be sufficient to transfer polarization inside the core region.

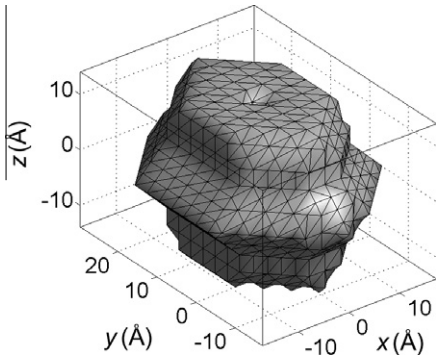

Fig. 6. A 3D representation of the "core" region around an electron pair calculated according to Eq. (24) with $\zeta = 5$. This example was calculated assuming a simple cubic lattice of protons, with a lattice parameter of 3.1 Å and its z-axis aligned with the direction of the external magnetic field. The electrons were positioned at [0,0,0] and [0,−4,0] on the lattice.

4.2. The SE and CE transitions

To follow the enhancement of the multi-nuclear core surrounding the electron pair we again restrict ourselves to nuclei with hyperfine coefficients that are smaller than the nuclear Zeeman frequency, $|A_{z,\varepsilon i}|, |A^{\pm}_{\varepsilon i}| \ll |\omega_n|$, for $\varepsilon = a, b$, $i = 1,\ldots,N_n$, and with nuclear dipolar interactions that are quenched by the hyperfine interaction. As long as we are removed from any spin-state degeneracies, and $|\delta\omega_e| \gg |D_{ab}|$, the eigenstates of the Hamiltonian stay almost equal to the product states, $|\chi^*_a, \chi^*_b; \chi^*_1, \ldots \chi^*_k \cdots, \chi^*_{N_n}\rangle$, with small state mixing due the hyperfine and electron dipolar interactions, as before. This state mixing, accompanied with small energy shifts, can again create small effective irradiation fields on the $ZQ_{\varepsilon i}$ and $DQ_{\varepsilon i}$ transitions. Each of these transitions is characterized by a single nuclear spin flip $\alpha_i \leftrightarrow \beta_i$ and simultaneously a single electron spin flip $\alpha_\varepsilon \leftrightarrow \beta_\varepsilon$ $\varepsilon = a,b$. Higher order MW matrix elements, involving more than a single nuclear transition, can be neglected in our case. Concentrating on one particular nucleus k and one electron a, the presence of all other nuclei $j \neq k$ generates a set of DQ_{ak} transitions with frequencies which are given to first order by

$$\omega_{DQ,ak} = \omega_a - \omega_n \pm \left(D_{ab} + \frac{1}{2}A_{z,bk}\right) + \frac{1}{2}\sum_{j\neq k}(\pm)_j A_{z,aj}. \tag{25}$$

The first ±1 sign is determined by the state α_b or β_b of electron b, and the other $(\pm1)_j$ signs by the α_j or β_j state. The effective MW fields for these transitions, which are responsible for SE-DNP, are all of the order of $(|\Delta A^{\pm}_k|/2\omega_n)\omega_1$ or $(|\delta A^{\pm}_k|/2\omega_n)\omega_1$. The expressions for the frequencies of the ZQ transitions are the same as in Eq. (25), except for $+\omega_n$ instead of $-\omega_n$.

A CE condition for spin k corresponds to a degeneracy between two states. For example the states $|\alpha_a, \beta_b; \chi_1, \ldots, \alpha_k, \ldots, \chi_{N_n}\rangle$ and $|\beta_a, \alpha_b; \chi_1, \ldots, \beta_k, \ldots, \chi_{N_n}\rangle$ become degenerate, to first order, when one of the following equalities are valid:

$$\delta\omega_e \cong \omega_n - \frac{1}{2}\sum_{j\neq k}(\pm)_j \delta A_{zj}. \tag{26}$$

At each of these CE conditions there is a single DQ_{ak} transition that has the same frequency as a SQ_b transition:

$$\omega_{SQ,b} = \omega_b \pm D_{ab} + \frac{1}{2}\sum_{j}(\pm)_j A_{z,aj}. \tag{27}$$

Other CE conditions occur when the frequencies of ZQ_{ak} and SQ_b transitions become equal. The effective MW fields of these DQ- or ZQ-CE transitions can again become about as strong as $\omega_1/\sqrt{2}$.

To show this effect we consider a spin system with two electron a, b, and three nuclei 1–3. For simplicity we assume that nuclei 1 and 2 interact only with electron a, and nucleus 3 only with electron b. The DQ_{a1} (down, black), DQ_{a2} (down, gray) and the SQ_b (up) spectra are schematically shown in Fig. 7, for $0 < A_{z,a1} < A_{z,b3} < A_{z,a2} < D_{ab}$. The four DQ_{a1} transitions are positioned at $\omega_a - \omega_n \pm D_{ab} \pm \frac{1}{2}A_{z,a2}$, while the four SQ_b transitions are positioned at $\omega_b \pm D_{ab} \pm \frac{1}{2}A_{z,b3}$. In the figure we show the DQ_{ak}–CE transition at

$$\omega_{DQ,ak} = \omega_a - \omega_n - D + \frac{1}{2}A_{z,a2} = \omega_b - D - \frac{1}{2}A_{z,b3} \tag{28}$$

overlapping with $\omega_{SQ,b}$. This corresponds to the $|\alpha_a, \beta_b; \alpha_1, \alpha_2, \beta_3\rangle$ to $|\beta_a, \beta_b; \beta_1, \alpha_2, \beta_3\rangle$ DQ transition, and to the $|\beta_a, \alpha_b; \beta_1, \alpha_2, \beta_3\rangle$ to $|\beta_a, \beta_b; \beta_1, \alpha_2, \beta_3\rangle$ SQ_b transition. In such a case the $|\alpha_a, \beta_b; \alpha_1, \alpha_2, \beta_3\rangle$ and $|\beta_a, \alpha_b; \beta_1, \alpha_2, \beta_3\rangle$ energy levels are degenerate, and the $\delta\omega_e = \omega_n - \frac{1}{2}(A_{z,a2} + A_{z,b3})$ CE condition is satisfied.

To conclude, the ZQ_{ak} and DQ_{ak} transitions of a particular electron-nuclear spin pair $a - k$ will be spread over a wide range of frequencies, due to the presence of the additional electron b and the nuclei $j \neq k$. For a given electron configuration some of these SE DQ or ZQ transitions can become DQ-CE or ZQ-CE transitions. Thus for some value of ω_{MW} the MW field can excite, for example, a band of DQ_{ak} transitions, of which only a part will be DQ_{ak}–CE transitions.

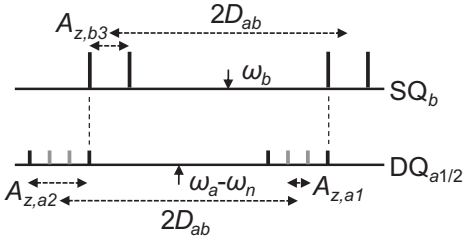

Fig. 7. Schematic representations of the positions of the DQ_{a1}, DQ_{a2} and SQ_b transitions of a five-spin system $\{e_a - e_b - n_{1-3}\}$. Nuclei 1 and 2 interact only with electron a, and nucleus 3 only with electron b, with $0 < A_{z,a1} < A_{z,b3} < A_{z,a2} < D_{ab}$. The frequency difference $\delta\omega_e$ was set equal to $\omega_n - \frac{1}{2}(A_{z,b3} + A_{z,a2})$. In the lower diagram the DQ_{a1} transitions are in black and the DQ_{a2}transitions in gray.

4.3. Ideal DNP experiments

We now consider the effect of MW irradiation on some or all of the DQ_{ai} transitions on the resulting nuclear polarization. When all of the DQ_{ai} or ZQ_{ai} transitions are saturated by the MW irradiation it can be shown that all polarizations become $|P_i(t)| = P_a(0)$, which corresponds to an ideal SE-DNP process. This can be derived using the same arguments as in Ref. [15] for a single electron. The same polarizations can be achieved when the MW irradiation excites only one of the electron dipolar DQ/ZQ satellites, as was discussed earlier.

We next discuss the effect of a MW irradiation exciting only a fraction f_i of the DQ_{ai} transitions in the case of SE-DNP. We demonstrate this here by assuming an irradiation of a single DQ_{ai} transition in a spin system of the form $\{e_b - e_a - n_1 - n_2\}$ that is far from any CE condition. The addition of one nucleus, denoted by 2, to the $\{e_b - e_a - n_1\}$ system induces a hyperfine spitting of the DQ_{a1} transitions, resulting in four DQ_{a1} transitions. Irradiation of only one of these transitions, for example $|\beta_a, \beta_b; \beta_1, \alpha_2\rangle - |\alpha_i, \beta_b; \alpha_1, \alpha_2\rangle$, will result in

$$\begin{aligned} p(\alpha^*_a, \beta^*_b; \beta^*_1, \alpha^*_2; t) &= \varepsilon_e p(\beta_a, \beta_b; \beta^*_1, \alpha^*_2; t) = \varepsilon_e p(\alpha^*_a, \beta^*_b; \alpha^*_1, \alpha^*_2; t) \\ &= \varepsilon^2_e p(\beta_a, \beta_b; \alpha^*_1, \alpha^*_2; t), \end{aligned} \tag{29}$$

in analogy with Eq. (19), and the action of $T^{-1}_{1,b}$ will result in

$$\begin{aligned} \varepsilon_e p(\alpha_a, \alpha_b; \beta^*_1, \alpha^*_2; t) &= \varepsilon^2_e p(\beta^*_a, \alpha^*_b; \beta^*_1, \alpha^*_2; t) \\ &= \varepsilon^2_e p(\alpha_a, \alpha_b; \alpha^*_1, \alpha^*_2; t) \\ &= \varepsilon^3_e p(\beta^*_a, \alpha^*_b; \alpha^*_1, \alpha^*_2; t). \end{aligned} \tag{30}$$

The overall population distribution here looks as if two of the four DQ_{a1}lines are saturated and we expect that the end polarizations become $P_i(t) = 0.5P_e(0)$. However, the $T^{-1}_{1,2}$ relaxation rate of nucleus 2 can enhance these end polarization. In contrast, irradiation on the DQ_{a2} transition may result in a decrease of the final polarization of nucleus 1. Both of these effects were shown for an $\{e_a - n_1 - n_2\}$system in Ref. [15]. The combined effect of all relaxation parameters and DQ_{ai} irradiation pathways is hard to envision exactly. This becomes even harder when considering the effects of MW irradiation on the SQ_b transitions close to the CE condition, or the effects of fast cross relaxation rates. However, in all cases the overall effect will result in some polarization enhancement.

4.4. A two-electron and three-nuclear spin system

To demonstrate the effect of the CE conditions on the nuclear enhancements we first consider a simple spin system with two interacting electrons, a and b, and three interacting nuclei 1–3. For simplicity we consider a spin system with all nuclei positioned close to the a electron, with the electrons and nucleus 1 having the same parameters as in the previous simulations (see Table 1). All other interactions and relaxations are given in the caption of Fig. 8. The steady state polarization of nucleus 1 as a function of ω_{MW} and the value of $\delta\omega_e$ is plotted in Fig. 8a. For simplicity we again consider only MW irradiation around $\omega_{MW} \approx \omega_a - \omega_n + |D_{ab}|$, and vary $\delta\omega_e$ in the vicinity of the CE condition $\delta\omega_e \approx \omega_n$, as was done in the previous contours. This complex contour demonstrates the interplay between the SE-DNP and the CE-DNP mechanisms for the same spin system. The four narrow vertical SE features in the contour are positioned at the DQ_{a1} transitions, with frequencies of $\omega_{MW} \simeq \omega_a - \omega_n - D_{ab} \pm A_{z,a2} \pm A_{z,a3}$. The four broad horizontal features correspond to CE conditions at $\delta\omega_e \simeq \omega_n \pm A_{z,a2} \pm A_{z,a3}$. Comparing this figure with Fig. 2b shows that when a single SE DQ_{a1} (black arrow in the figure, for example) or a DQ_{a1}–CE transition (lower white arrow, for example) is affected the polarization is greatly reduced. However, when several transitions are affected, for example due to off-resonance irradiation on the DQ_{a1}–CE and on-resonance irradiation on the SE DQ transition (upper white arrow, for example) the polarization is increased. This can also be seen in Fig. 8b, where the MW irradiation strength was increased to $\omega_1/2\pi = 0.5$ MHz. We note that the resulting polarization can increase due to a decrease in $T^{-1}_{1,\varepsilon 1}$ or $T^{-1}_{1,1}$ or an increase in $T^{-1}_{1,\varepsilon j}$ or $T^{-1}_{1,j}$ of $j = 2, 3$.

Polarization build up curves for the five-spin system are shown in Fig. 8c. These curves are evaluated for the three conditions which were mentioned earlier and that are indicated by the arrows in Fig. 8a: (i) a single SE DQ_{a1} transition is irradiated on-resonance (dashed black line); (ii) a single DQ_{a1}–CE transition is irradiated on-resonance (solid black line); and (iii) a single SE DQ_{a1} transition is irradiated on-resonance simultaneously with a DQ_{a1}–CE transition off-resonance (solid gray line). A MW irradiation of $\omega_1/2\pi = 0.1$ MHz was used here, as in Fig. 8a. The initial buildup time is shown in the insert of this figure. When only the SE mechanism is involved the polarization buildup is gradual, while for the CE mechanism there is an initial increase in the polarization. In all cases the steady state is reached in the time scale of T_{1n}. This is due to the contribution of the $T_{1,j}$ and $T_{1,\varepsilon j}$ relaxation process of nuclei $j = 2, 3$ to the polarization of nucleus 1, when only a part of the DQ_{a1} transitions are affected by the MW irradiation.

4.5. A two-electron and multi-nuclear spin system

We next examine the DNP mechanism in a system composed of two coupled electrons, a and b, and a large number of core nuclei $N_n \gg 1$. The nuclear polarizations of this system can not be simulated using the master equation, but we will try to estimate the influence of the presence of nuclei $j \neq k$ on the polarization enhancement of one particular nucleus k. The DQ_{ak} and ZQ_{ak} transitions, as well as the possible DQ_{ak}–CE and ZQ_{ak}–CE transitions, are spread over a frequency range determined by the hyperfine coupling coefficients of all other nuclei A_{aj} with $j \neq k$, as given in Eq. (25). As a result only a fraction f_k of all DQ_{ak} and ZQ_{ak} transitions are affected by a MW irradiation field. Although this fraction is not the only factor determining the enhancement of nucleus k, as was explained above, it clearly plays a significant role. Once again, for $f_k = 1$ we can expect substantial enhancements, up to full polarization transfer $|P_k(t)| = P_{a,b}(0)$, by the SE process, when $T^{-1}_{1,k}, T^{-1}_{DQ/ZQ} \ll T^{-1}_{1e}$. On the other hand when f_k approaches zero the k-spin enhancement will also become zero. This, in addition to the results of Fig. 8, indicates that globally $P_k(t)$ will increase with increasing f_k. From the earlier discussion we can however expect that the spin lattice relaxations of the electrons and nuclei $j \neq k$ will tend to increase the polarization $P_k(t) > f_k P_e(0)$, while

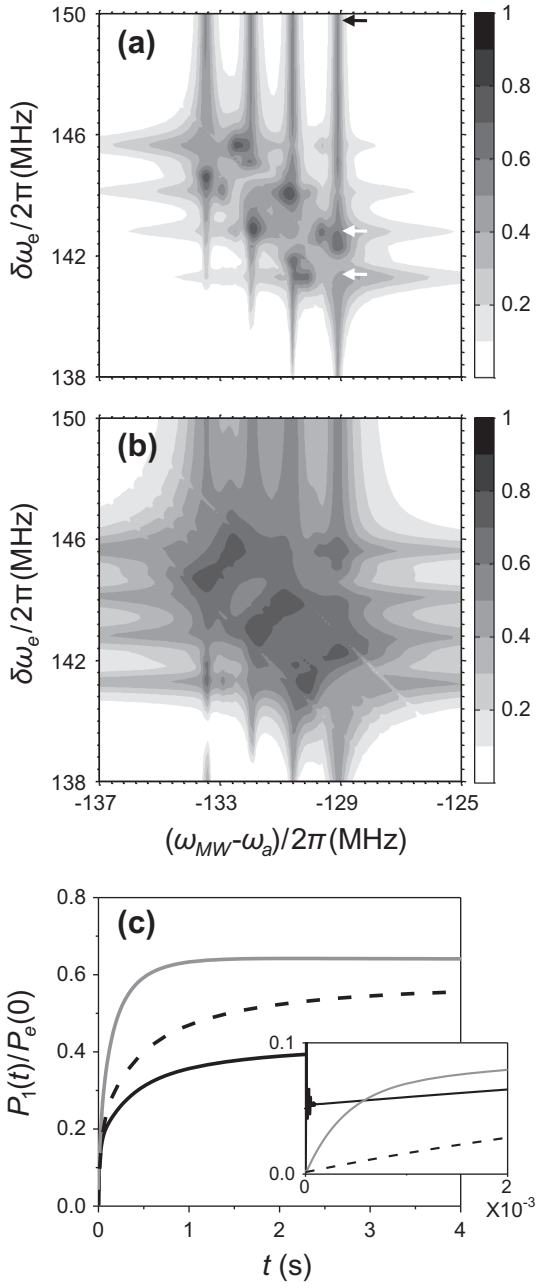

Fig. 8. The steady state nuclear polarization of nucleus 1, $P_1(t)$, in a five-spin system $\{e_a - e_b - n_{1-3}\}$ during a cw MW irradiation as a function of the MW frequency ω_{MW} and the difference between the electron frequencies $\delta\omega_e$. During the simulations the MW intensity was set equal in (a) to $\omega_1/2\pi = 0.1$ MHz and in (b) to 0.5 MHz. In (c) the temporal evolution of $P_1(t)$ with a MW frequency at $\omega_{MW}/2\pi = -129.1$ MHz is shown for $\delta\omega_e/2\pi = 141.3$ MHz (solid black line), 142.8 MHz (solid gray line) and 150 MHz (dashed black line), as indicated by the arrows in contour (a). The MW intensity was set at $\omega_1/2\pi = 0.1$ MHz. The two electrons and nucleus 1 where positioned as described in Table 1 (for $n = 1$), resulting in the same spin-interaction strength. Nuclei 2,3 were added to this spin system at positions [2.8,0,0.6] Å and [−1.2,0,4.3] Å relative to electron a. This resulted in $A_{z,a2}/2\pi = 2.85$ MHz, $A_{z,a3}/2\pi = -1.5$ MHz, $A_{z,b2}/2\pi = 0.02$ MHz, $A_{z,b3}/2\pi = 0.03$ MHz, $A^{+}_{a2}/2\pi = 2.11$ MHz, $A^{+}_{a3}/2\pi = 0.77$ MHz, $A^{+}_{b2}/2\pi < 0.01$ MHz, $A^{+}_{b3}/2\pi = 0.04$ MHz and $|d_{i<j}| < 8$ kHz. The cross relaxation times $T_{1,aj}$ were set equal to 2.5 s, 0.2 s, and 2.5 s for $j = 1, 2, 3$, respectively, and $T_{1,bj}$ equal to 1000 s. All other interaction and relaxation parameters are given in Table 1.

inefficient MW irradiation, and possibly also irradiation of SQ transitions and partial excitation of f_j transitions, will diminish it.

To estimate the dependence of f_k on the MW frequency and on the value of $\delta\omega_e$, we will assume that the spread of the DQ_{ak}, ZQ_{ak} and SQ_b transitions of the spin system are solely determined by the secular terms of the hyperfine interaction and the dipolar interaction between the two electrons. The evaluation of f_k was done in three steps:

(i) In the first step we calculated the normalized number of DQ_{ak} transitions, $n_{DQ,ak}(\omega_{DQ})$, around one of the dipolar satellites such as $\omega_{DQ} \approx \omega_a - \omega_n + |D_{ab}|$. These transitions are of the form $|\beta_a,\beta_b;\ \beta_k,\ \chi_{j\neq k}\rangle - |\alpha_a,\ \beta_b;\ \alpha_k,\ \chi_{j\neq k}\rangle$, for all $j \neq k$ and $\chi_{j\neq k} = \alpha_j, \beta_j$. An example of a $n_{DQ,ak}$ spectrum is shown in Fig. 9a for a cubic lattice of nuclei around two electrons, as defined in the figure caption.

(ii) In the second step we determined for a given value of ω_{DQ} and $\delta\omega_e$ (in the vicinity of ω_n) which part of these transitions are overlapping with SQ_b transitions, resulting in the DQ_{ak}–CE transitions. The result of this calculation is shown in Fig. 9b, where each point in the contour indicates the normalized number of DQ_{ak} transitions that have become DQ_{ak}–CE transitions for the specific ω_{DQ} and $\delta\omega_e$ values.

(iii) In the last step we calculated the value of $f_k(\omega_{MW}, \delta\omega_e)$ as a function of the MW frequency ω_{MW} and of $\delta\omega_e$. Here we assumed that SE DQ_{ak} and DQ_{ak}–CE transitions in the range $\omega_{DQ,ak} = \omega_{MW} \pm \frac{1}{2}\delta\omega_{MW}$ contribute to $f_k(\omega_{MW},\ \delta\omega_e)$. The width $\delta\omega_{MW}$ depends on the MW field strength and the relaxation rates $\left(\omega_{1,kk'}, T^{-1}_{1kk'}, T^{-1}_{2,kk'}\right)$, and will therefore vary significantly between the two types of transitions. For each $\delta\omega_e$ value only DQ_{ak}-CE transitions in a range $\delta\omega_e \pm \frac{1}{2}\delta\omega_{CE}$ contribute to $f_k(\omega_{MW}, \delta\omega_e)$, while all other DQ_{ak} transitions are counted as SE transitions.

Fig. 9c shows the value of f_k for different ω_{MW} and $\delta\omega_e$ values. To obtain this contour we chose a rather high value of $\delta\omega_{CE} = 1$ MHz, and the $\delta\omega_{MW}$ values 1 MHz and 20 MHz for the SE DQ_{ak} and DQ_{ak}–CE transitions, respectively. For example, the area between the dashed lines in this Fig. 9b indicate the part of the DQ_{ak}–CE transitions that contribute to $f_k(\omega_{MW},\delta\omega_e)$ for the ω_{MW} and $\delta\omega_e$ values marked by the arrows. The SE DQ_{ak} and DQ_{ak}–CE transitions affected by the MW field are shown schematically by the black and gray areas in Fig. 9a, respectively.

This calculation results in a rather low maximum value for f_k of about 12%. This indicates that to achieve higher polarizations it is worthwhile to dilute the spin system, and in particular of nuclei in proximity to the electrons.

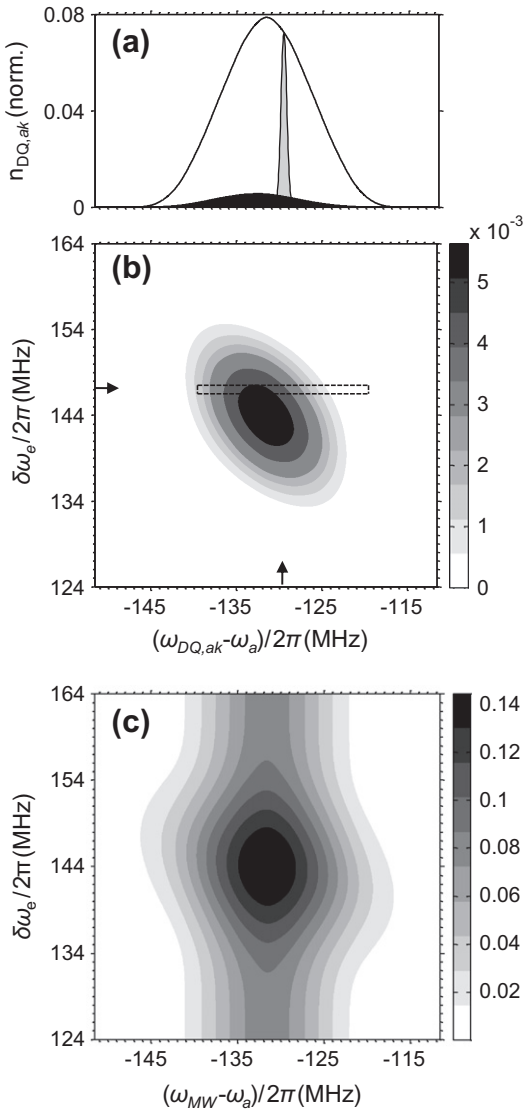

Fig. 9. The fraction of DQ_{ak} transitions $f_k(\omega_{MW}, \delta\omega_e)$ affected by MW irradiation. This was calculated for a spin system composed of two electrons a and b surrounded by a cubic lattice of protons with a lattice constant of 3.1 Å of size $13 \times 17 \times 13$ (x,y,z) spins. The external magnetic field is pointing in the z direction. The electrons were put in the lattice at positions [0,±2,0], and the nucleus k at [0,5,0]. In (a) the $n_{DQ,ak}(\omega_{DQ,ak})$ spectrum (black line) is composed of all DQ_{ak} transitions with frequencies $\omega_{DQ,ak}$ close to $\omega_a - \omega_n - D_{ab}$. The normalized number of DQ_{ak} transitions that become DQ_{ak}–CE transitions is shown in (b), for different $\delta\omega_e$ values. The calculation was performed by taking into account successively the contribution of the secular part of the hyperfine interaction of each nucleus. The changes in the DQ_{ak} spectrum were calculated using Eq. (25). The frequencies at which these transitions satisfy the CE condition, and overlap with a SQ_b transition, were calculated using Eq. (26). The frequency of these new transitions were put on a frequency grid with a resolution of 20 kHz. The fraction f_k of the DQ_{ak} transitions that are excited by a MW irradiation at ω_{MW} for different $\delta\omega_e$ values is drawn in (c), with the calculation performed as described in the text. The dashed area in (b) and the black and gray areas in (a) show an example of this calculation, as indicated in the text.

5. Discussion

In this publication we have characterized the spin dynamics of CE-DNP processes in systems containing a pair of coupled electrons interacting with a set of neighboring core nuclei. Here we have assumed that the dipole–dipole interactions between these nuclei are quenched by the hyperfine interactions. This study is a continuation of our earlier investigation dealing with SE-DNP processes in systems composed of a single electron interacting with a set of neighboring core nuclei. The purpose of both studies has been to determine the basic theoretical concepts describing the SE-DNP and CE-DNP mechanisms by using quantum mechanical simulations of model systems with an emphasis on the influence of the spin relaxation processes essential for the polarization enhancements. In these studies we did not intend to analyze specific experimental results, but rather set a stage for the interpretation of future DNP experiments on solids.

Using the same theoretical framework, we made a clear distinction between the spin behavior in the two model systems $\{e_a - n_{N_n}\}$ and $\{e_a - e_b - n_{N_n}\}$. The spin dynamics of the DNP process in the two electron case varies from the one electron case when part of the DQ_{an} or ZQ_{an} transitions of a spin pair $\{e_a - n\}$ overlaps with SQ_b transitions of electron b. As a result the effective MW fields on the overlapping DQ_{an} transitions increase and the bandwidth of the frequency profile of the DNP polarization broadens. Similar as for SE-DNP, in the case of CE-DNP the electron

spin–lattice relaxation is essential for achieving full polarization transfer. Due to the large effective MW fields in CE-DNP the nuclear polarization build up curves differ from those in SE-DNP. When irradiating on-resonance the time it takes to reach saturation of the DQ–CE or ZQ–CE transitions is typically faster than the electron relaxation time $T_{1,e}$, and the time-scale of the steady state polarization build-up will be in the order of this relaxation time. Additionally, the large effective MW fields can enable efficient irradiation of DQ-CE transitions many MHz off-resonance. At low MW powers or far off-resonance the steady state polarization buildup time scales will become dependent on cross relaxation times $T_{1,DQ/ZQ}$, which in the CE–DNP case are still in the order of $T_{1,e}$. This is in contrast to the SE-DNP mechanism, where the steady state buildup time-scale can become very sensitive to the effective MW fields and off-resonances and can reach the nuclear spin–lattice relaxation times. It should be noted that these differences are relevant only when discussing the core nuclei. The build up of bulk polarization is related to the DNP-assisted spin diffusion processes which will be discussed elsewhere.

The complexity of the spin dynamics in multi-nuclear systems surrounding the electrons is a result of the fact that the DQ and ZQ transitions of each electron-nuclear spin pair are split by the hyperfine interaction of all other nuclei. If the MW irradiation affects only a small part of these transitions the DNP enhancement will be significantly reduced. Additionally, the CE condition is split, such that when the electrons are at one of the CE conditions only a small fraction of the DQ or ZQ transitions are CE transitions. This therefore suggests that the DNP enhancement of the core nuclei is only partially driven by CE-DNP processes, and that the total enhancement must be characterized by a combination of SE-DNP and CE-DNP processes.

Various aspects of the DNP spin dynamics were not discussed here and they have to be investigated in future DNP studies. For example, during our calculations we used relaxation parameters that were not derived from basic relaxation theory, but were chosen by considering values similar to the ones reported in the literature. It will however be necessary to examine the various relaxation mechanisms involved in the DNP enhancement processes and use or derive explicit expressions for the relaxation rates originating from fluctuating interactions such as hyperfine and dipolar interactions in the solid state [27]. In addition electron relaxation mechanisms, such as phonon limited direct and Raman relaxation processes [28], should also be incorporated in these derivations.

Another issue that needs additional attention is the DNP-assisted spin diffusion process polarizing the bulk. As mentioned earlier we refrained here from dealing with these spin diffusion processes [17]. These are however essential for the understanding of the experimental data and we are currently in the process of addressing these mechanisms for the CE-DNP case. The growth of polarization of a bulk nucleus depends on the effective MW fields of the spin system and their contributions to that particular nucleus. These effective fields are distributed over transitions between the eigenstates of the whole spin system and are determined by the diagonalization of the core-bulk and bulk-bulk dipolar interactions. Large effective MW fields on the core nuclei will result in larger fields driving the bulk polarization, and as a result more bulk nuclei will be effectively polarized. These issues must be elaborated on further and must be addressed when analyzing experimental DNP results.

In practice many DNP experiments are performed on amorphous glasses containing randomly oriented radicals. Thus for example during DNP experiments using nitroxide radicals we encounter broad powder EPR line shapes, induced by g-tensor anisotropies, and MW irradiation fields that only excite transitions close to resonance. This means that only a fraction of the electrons in the sample contribute actively to the nuclear polarization enhancement. In the case of bi-radicals in static samples their random orientation and the corresponding SQ transition frequencies of the two electron spins strongly reduces the number of electron pairs in the sample that can directly contribute to the CE-DNP processes. When mono-radicals are the source of the paired electrons in the system, their concentration determines the percentage of electrons that contribute to CE-DNP enhancement. Thus in both cases, when CE-DNP is the major polarization mechanism in a sample, the sphere of enhanced bulk nuclei around an electron pair at a CE condition must be large relative to the same sphere around electrons that are not at a CE condition. While in every powder experiment both DNP processes are simultaneously active, the CE-DNP process will determine the overall polarization only when the small fraction of "CE spin pairs" dominate the larger fraction of "SE electrons" in enhancing the bulk.

Many electrons in the sample are not actively involved in the DNP enhancement process for any MW irradiation when the EPR powder line shape is broad. Then a question that must be answered is in what manner do these non-DNP active electrons influence the SE-DNP and CE-DNP processes in the sample. Many of these electrons interact with the active electrons and cause a broadening of the DQ spectra. Perhaps we would then expect that this broadening will reduce the MW excitation efficiency and would reduce the final nuclear enhancement. This however is not the case, as will be shown in a later publication. When considering some aspects of the TM DNP process, the non-directly DNP active electrons support the overall polarization enhancement process.

Describing DNP results involving nitroxide radicals as the unpaired electron source, we must take into account the presence of the ^{14}N nuclei that are strongly hyperfine coupled to each electron. A careful investigation of the influence of the nitrogen atoms on the DNP processes is then necessary. This was not discussed here in order not to complicate the present derivations. A comment we must however make is that for short spin–lattice relaxation times of the ^{14}N nuclei, irradiation on one of the three satellite bands of the DQ transitions, corresponding to the nitrogen hyperfine splitting, can result in nuclear polarizations that are significantly higher than $0.3P_e(0)$.

Finally we should mention the influence of sample spinning on the DNP processes encountered in MAS-DNP in solid state NMR [29]. Due to this sample rotation, the MW irradiation excites large parts of the DQ, ZQ and EPR transitions of the electrons in the amorphous powder samples and we can expect a significant increase in the number of electrons contributing to the total bulk polarization. These effects and others must be formulated and taken into account when describing the SE- and CE-DNP mechanism in rotating solids.

Acknowledgments

We mention here fruitful discussions with Dr. Walter Köckenberger concerning the relaxation mechanisms that enable efficient DNP experiments. The work was supported by the German-Israeli Project Cooperation of the DFG through a special allotment by the Ministry of Education and Research (BMBF) of the Federal republic of Germany and this research was made possible in part by the historic generosity of the Harold Perlman Family. S.V. holds the Joseph and Marian Robbins Professorial Chair in Chemistry.

References

[1] D. Hall, D. Maus, G. Gerfen, S. Inati, L. Beccera, F. Dahlquist, R.G. Griffin, Science 276 (1997) 930–932.
[2] M. Rosay, J. Lansing, K. Haddad, W. Bachovchin, J. Herzfeld, R. Temkin, R.G. Griffin, J. Am. Chem. Soc. 125 (2003) 13626–13627.

[3] J. Ardenkjr–Larsen, B. Fridlund, A. Gram, G. Hansson, L. Hansson, M. Lerche, R. Servin, M. Thaning, K. Golman, Proc. Natl. Acad. Sci. USA 100 (2003) 10158–10163.
[4] M.E. Merritt, C. Harrison, C. Storey, F.M. Jeffrey, A.D. Sherry, C.R. Malloy, Proc. Natl. Acad. Sci. 104 (2007) 19773–19777.
[5] C. Jefferies, Phys. Rev. 106 (1957) 164–165.
[6] A. Abragam, W.G. Proctor, Comptes Rendus Hebdomadaires des Seances de l'Academie des Sciences 246 (1958) 2253–2256.
[7] A.V. Kessenikh, V.I. Lushchikov, A.A. Manenkov, Y.V. Taran, Sov. Phys. Solid State 5 (1963) 321–329.
[8] A.V. Kessenikh, A.A. Manenkov, G.I. Pyatnitskii, Sov. Phys. Solid State 6 (1964) 641–643.
[9] C.F. Hwang, D.A. Hill, Phys. Rev. Lett. 19 (1967) 1011–1013.
[10] A. Abragam, M. Goldman, Nuclear Magnetism: Order and Disorder, Clarendon, Oxford, 1982.
[11] A. Abragam, M. Goldman, Rep. Prog. Phys. 41 (1978) 395–467.
[12] M.J. Duijvestijn, R.A. Wind, J. Smidt Phys. 138B (1986) 147–170.
[13] C.T. Farrar, D.A. Hall, G.J. Gerfen, J. Chem. Phys. 114 (2001) 4922–4933.
[14] D.S. Wollan, Phys. Rev. B 13 (1976) 3671–3685.
[15] Y. Hovav, A. Feintuch, S. Vega, J. Magn. Reson. 207 (2) (2010) 176–189.
[16] A. Van Der Drift, A. Karabanov, I. Kuprov, W. Köckenberger, Exper. Nucl. Magn. Res. Conff., 2011.
[17] Y. Hovav, A. Feintuch, S. Vega, J. Chem. Phys. 134 (7) (2011) 074509.
[18] C.F. Hwang, D.A. Hill, Phys. Rev. Lett. 18 (1967) 110–112.
[19] K.N. Hu, H.H. Yu, T.M. Swager, R.G.J. Griffin, Am. Chem. Soc. 126 (2004) 10844.
[20] C. Song, K.N. Hu, C.G. Joo, T.M. Swager, R.G. Griffin, J. Am. Chem. Soc. 128 (2006) 11385–11390.
[21] K.N. Hu, PhD, MIT, 2006.
[22] K.N. Hu, G.T. Debelouchina, A.A. Smith, R.G. Griffin, J. Chem. Phys. 134 (2011) 125105.
[23] A. Schweiger, G. Jeschke, Principles of Pulse Electron Paramagnetic Resonance, Oxford University Press, New York, 2001.
[24] C.P. Slichter, Principles of Magnetic Resonance, Springer, Berlin, Heidelberg, 1990.
[25] S. Stoll, B. Epel, S. Vega, D. Goldfarb, J. Chem. Phys. 127 (2007) 164511.
[26] J. van Houten, W.Th. Wenckebach, N.J. Poulis, Physica B+C 92 (1977) 210–220.
[27] A. Abragam, Principles of Nuclear Magnetism, Oxford University Press, New York, 1961.
[28] A. Abragam, B. Bleaney, Electron Resonance of Transition Ions, Oxford University Press, New York, 1970.
[29] T. Maly, G.T. Debelouchina, V.S. Bajaj, K.-N. Hu, C.-G. Joo, M.L. Mak–Jurkauskas, J.R. Sirigiri, P.C.A. van der Wel, J. Herzfeld, R.J. Temkin, R.G. Griffin, J. Chem. Phys. 128 (2008) 052211.